
Recent results of laser spectroscopy experiments of pionic helium atoms at PSI

M. Hori^{1*}, H. Aghai-Khozani^{1†}, A. Sótér^{1‡}, A. Dax² and D. Barna^{3§}

1 Max-Planck-Institut für Quantenoptik, Hans-Kopfermann-Strasse 1, D-85748 Garching, Germany

2 Paul Scherrer Institut, CH-5232 Villigen, Switzerland

3 CERN CH-1211, Geneva, Switzerland

* Masaki.Hori@mpq.mpg.de

† Current address: McKinsey and Company, Munich, Germany

‡ Current address: ETH Zürich, IPA, Zurich, Switzerland

§ Current address: Institute for Particle and Nuclear Physics, Wigner Research Centre for Physics, Budapest, Hungary

January 4, 2021

PAUL SCHERRER INSTITUT



Review of Particle Physics at PSI

doi:[10.21468/SciPostPhysProc.2](https://doi.org/10.21468/SciPostPhysProc.2)

Abstract

A review of a recent experiment carried out at PSI involving laser spectroscopy of metastable pionic helium ($\pi^4\text{He}^+ \equiv \pi^- + {}^4\text{He}^{2+} + e^-$) atoms is presented. An infrared transition $(n, \ell) = (17, 16) \rightarrow (17, 15)$ at a resonance frequency of $\nu \approx 183760$ GHz was detected.

26.1 Introduction

Metastable pionic helium is a neutral exotic atom [1–4] that contains a helium nucleus with an electron in the ground state, and a negatively-charged pion (π^-) occupying a state having high principal and orbital angular momentum quantum numbers of around $n \sim \ell + 1 \sim 16$. These states have nanosecond-scale lifetimes against the competing cascade processes of π^- nuclear absorption and $\pi^- \rightarrow \mu^- + \bar{\nu}_\mu$ decay. This longevity arises because the π^- orbitals have very small overlap with the nucleus, and so the rates of electromagnetic cascade processes involving the rapid deexcitation of the π^- , such as Auger and radiative decays are significantly reduced. It should therefore be possible to carry out laser spectroscopy [5, 6] of $\pi^4\text{He}^+$ which would constitute the first such measurement of an exotic atom that contains a meson. Such an experiment would conclusively show the heretofore hypothetical existence of $\pi^4\text{He}^+$. By comparing the atomic frequencies measured by laser spectroscopy with the results of quantum electrodynamics (QED) calculations, the π^- mass [7–9] can, in principle, be determined with a high precision. This can help set upper limits on constraints on the muon antineutrino mass by laboratory experiments [10]. Some upper limits may also be set on any exotic force [11–15] that involves the π^- , as has been done in the case of antiprotonic helium ($\bar{p}\text{He}^+ \equiv \bar{p} + \text{He}^{2+} + e^-$) atoms [16–26]. Unlike the $\bar{p}\text{He}^+$ case, the atomic structure of $\pi^4\text{He}^+$ contains no hyperfine structure that arises from the spin-spin interaction between the spin-0 π^- and ${}^4\text{He}$ nucleus [27, 28].

The existence of πHe^+ atoms has been inferred in an indirect way from four experiments [29–33] that were initially carried out using early synchrocyclotron facilities [34, 35] and liquid helium bubble chambers [36]. All these experiments observed that some π^- coming to rest in helium targets have an anomalously long lifetime. Comparisons of the data with the theoretical

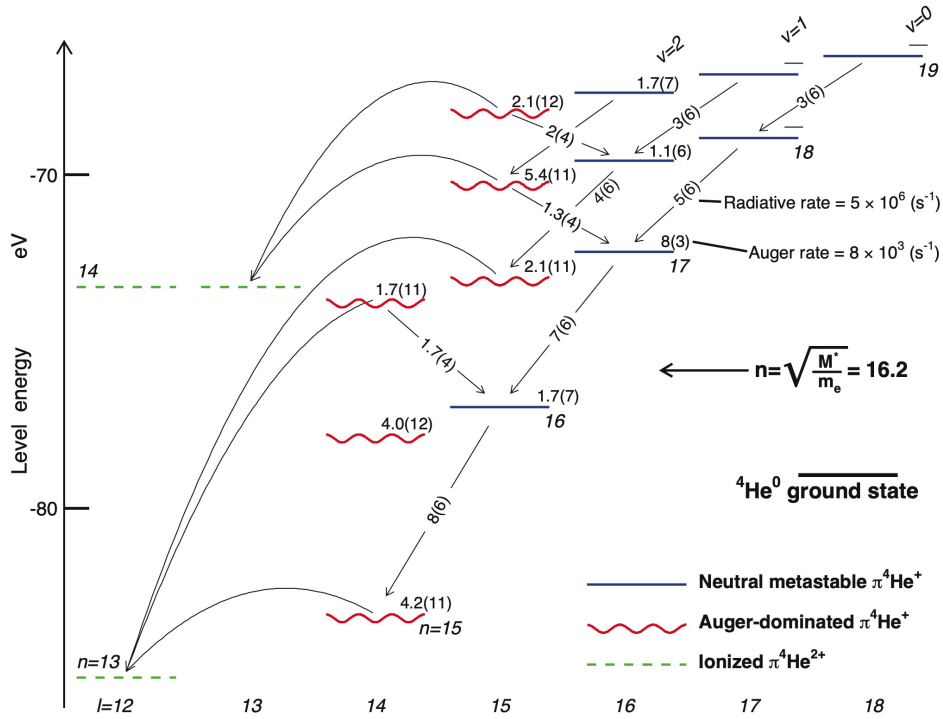


Figure 26.1: An energy level diagram of the exotic atom $\pi^4\text{He}^+$. The theoretical absolute energy of the states (n, ℓ) are plotted relative to the three-body-breakup threshold. The wavy lines indicate Auger-dominated states that have picosecond-scale lifetimes, and the solid lines show metastable levels with lifetimes of > 10 ns. The Auger decay rates are indicated in s^{-1} . The dashed lines show the $\pi^4\text{He}^{2+}$ ionic states which are formed after Auger electron emission. The curved arrows indicate the Auger transitions that have minimum $|\Delta\ell_A|$. The radiative transitions $(n, \ell) \rightarrow (n-1, \ell-1)$ and $(n, \ell) \rightarrow (n-1, \ell+1)$ are shown using straight arrows, with the corresponding decay rates indicated in s^{-1} . From Ref. [6].

42 calculations have been difficult, however, as some sets of calculated decay rates of $\pi^4\text{He}^+$
 43 states have differed from each other by 1–2 orders of magnitude [2, 4, 6]. The transitions
 44 between short-lived states with a small principal quantum number n_i for singly charged, two-
 45 body pionic helium ($\pi^4\text{He}^{2+} \equiv \pi^- + {}^4\text{He}^{2+}$) ions have been measured by X-ray fluorescence
 46 spectroscopy with a precision of $\sim 10^{-4}$ in the 1970's or earlier [37–39]. The atomic lines of
 47 $\pi^4\text{He}^+$ were not detected until very recently [5].

48 26.2 Experimental method

49 In the recent PSI experiment, laser pulses excited a transition from a pionic state of the neutral
 50 atom that had a nanosecond-scale lifetime, to a state with a picosecond-scale lifetime against
 51 Auger decay [6] (Figure 26.1). A two-body $\pi^4\text{He}^{2+}$ ion was formed after Auger emission of
 52 the 1s electron. The ion was then promptly destroyed by collisions with other helium atoms,
 53 which caused Stark mixing between the Rydberg and low ℓ orbitals of the ion [38, 40] as
 54 well as other possible effects [41]. This Stark mixing led to the absorption of the π^- by the
 55 nucleus. The resonance condition between the laser beam and the $\pi^4\text{He}^+$ atom was detected
 56 as a peak in the rates of neutrons, protons, and deuterons. This peak was superimposed on
 57 a background containing other $\pi^4\text{He}^+$ atoms that decayed spontaneously with a lifetime of

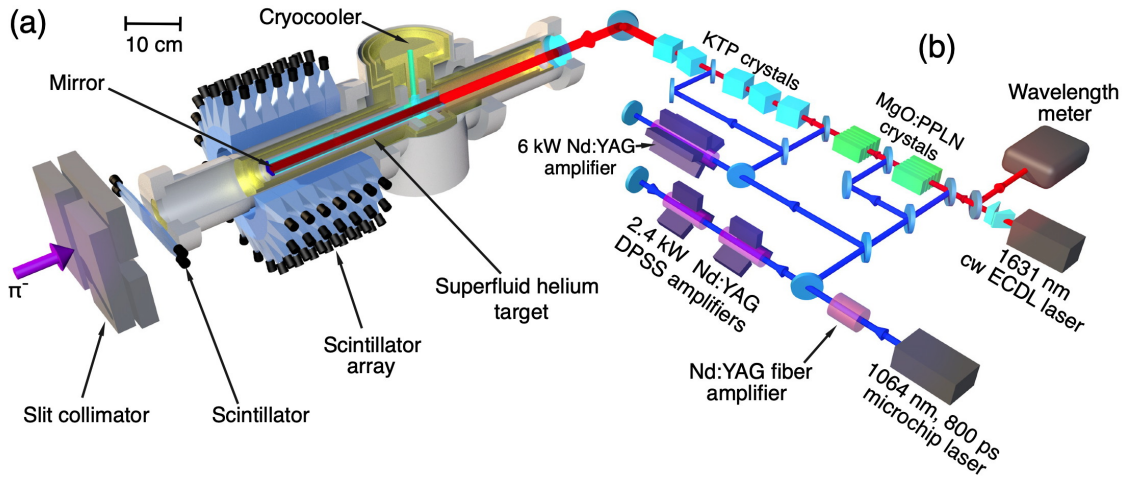


Figure 26.2: (a): Schematic showing the layout of the target used in the experiment. The π^- beam passed through a scintillation counter and then came to rest in the cryogenic helium target. This resulted in the production of $\pi^4\text{He}^+$ atoms. The atoms are irradiated with $\Delta t = 800$ ps long laser pulses with energy $E = 10$ mJ and wavelength $\lambda \approx 1631$ nm. The proton, neutron, and deuteron fragments that emerge from the π^- absorption are detected by 140 plastic scintillation counters that surround the target. (b): Schematic layout of the laser system, see text. From [5].

58 around ~ 7 ns [6, 33].

59 This experiment used the πE5 beamline [42] that provided a π^- beam that had a momen-
 60 tum between 83 and 87 MeV/c, and an average intensity of $N_\pi = (2 - 3) \times 10^7 \text{ s}^{-1}$. A Wien
 61 filter was placed upstream of the target. This filter diverted most of the contaminant e^- that
 62 arrived at a rate $> 3 \times 10^9 \text{ s}^{-1}$ into the blades of a slit collimator made of steel. The purified π^-
 63 beam was focused into an elliptical beam spot that had a full-width-at-half-maximum (FWHM)
 64 horizontal size of 23 mm and vertical size of 15 mm. For this a pair of quadrupole magnets
 65 provided by the CERN magnet group was used. The π^- beam passed through a plastic scintil-
 66 lator plate that had a thickness $t_d = 4.7$ mm. The plate was segmented into four sections with
 67 each section having a size of 20×20 mm. The beam then entered the experimental target.

68 The correlations between the arrival times t_a and energy depositions ΔE of hits that oc-
 69 curred in the scintillator plates at the entrance of the experimental target are shown in the
 70 contour plot of Figure 26.3 (a). The π^- arrived at the target in bursts spaced by regular in-
 71 tervals $\Delta t = 19.75$ ns. This arose from the $f_a = 50.63$ MHz radiofrequency of the 590 MeV
 72 cyclotron, with each RF cycle containing on average $N_\pi/f_a \approx 0.4 - 0.6 \pi^-$. The π^- arrival
 73 events which are located in the rectangular area indicated by broken lines were distinguished
 74 from μ^- and e^- in the beam by the time-of-flight methods and the estimated ΔE value of 2.6
 75 MeV for π^- in the scintillator plate.

76 We assumed that a 2.3% fraction of the π^- that were able to come to rest in the superfluid
 77 helium target (Figure 26.2 (a)) with a length of 150 mm, diameter of 42 mm, and a temper-
 78 ature of $T = 1.7$ K formed the metastable variant of the atoms [33]. A laser beam that had a
 79 diameter of $d = 25$ mm, a pulse length of $\Delta t = 800$ ps, pulse energy $E = 10$ mJ, repetition
 80 rate $f_r = 80.1$ Hz and wavelength $\lambda \approx 1631$ nm entered the target. The beam irradiated
 81 $> 60\%$ of the $\pi^4\text{He}^+$ produced in the target. The implied production rate of the pionic atoms
 82 of $> 3 \times 10^5 \text{ s}^{-1}$ ensured that we retain a probability of coincidence of around 10^{-3} for a laser
 83 pulse to irradiate a $\pi^4\text{He}^+$ atom.

84 The nuclear fragments that emerged from the absorption of π^- tended to follow tranjec-

85 tories that were anticollinear [6, 43, 44] with a typical kinetic energy of a few tens of MeV.
 86 The arrival times t_a and the energy depositions ΔE of the fragments were measured (Fig-
 87 ure 26.3 (b)) by an array containing 140 plastic scintillation counters with size $40 \times 35 \times 34$
 88 mm^3 . These counters covered a solid angle of $\sim 2\pi$ steradians seen from the target. The
 89 size of the scintillation counters was chosen so that the detection efficiency for $E \geq 25$ MeV
 90 neutrons was significant ($< 10\%$) [6] while simultaneously achieving the discrimination con-
 91 dition which rejected most of the background e^- from either μ^- decay or the particle beam.
 92 The background e^- deposited an average energy $\Delta E = 6 - 8$ MeV. Monte Carlo simulations
 93 indicated that most of these events could be removed by rejecting those events an energy de-
 94 position of $\Delta E < 20 - 25$ MeV. The waveform [45–47] of the signal from the counters were
 95 recorded during each laser pulse arrival by using waveform digitizers that had sampling rates
 96 of $f = 3.06 \text{ Gs}\cdot\text{s}^{-1}$. We did this by developing a custom readout system, which used the DRS4
 97 chip which is an application-specific integrated circuit (ASIC) that was based on switched ca-
 98 pacitor arrays [48, 49]. An earlier version of the electronics based on the DRS4 ASIC was used
 99 in an experiment to determine upper limits on the annihilation cross sections of antiprotons of
 100 kinetic energy $E \approx 125$ keV on thin target foils [46, 50], the results of which were compared
 101 with the cross sections measured at higher energies $E = 5.3$ MeV [51, 52].

102 Figure 26.3 (b) shows a $t_a - \Delta E$ contour plot of hits on the scintillator array surrounding the
 103 target. We selected those events that were within the area indicated by the broken lines. This
 104 removed most of the background e^- as well as fission products with low velocities. The blue
 105 time spectrum of Figure 26.3 (c) shows the distribution of scintillator hits that were measured
 106 without any laser beam irradiating the atoms. The consecutive π^- arrivals at $t = 0$ and at
 107 $t = 19.75$ ns produced a pair of peaks in the spectrum that contained the $> 97\%$ majority of
 108 π^- that underwent nuclear absorption immediately after arriving in the target. The fraction
 109 $(2.1 \pm 0.7)\%$ that remained constituted a spectrum with a decay lifetime of $\tau = 7 \pm 2$ ns in the
 110 intervals between the arrivals of π^- . This approximately agreed with the results of a Monte
 111 Carlo simulation [6] of the expected signal, and with an experiment carried out previously [33]
 112 using a target filled with liquid helium.

113 The laser pulses that reached the experimental target at a time $t = 9$ ns after the ar-
 114 rival of π^- had a timing jitter of typically $\Delta t \leq 1$ ns. These laser pulses were produced by
 115 an injection-seeded, optical parametric generator (indicated as OPG in Figure 26.2(b)) and
 116 amplifier (OPA) laser system. We constructed a diode-pumped solid state (DPSS) neodymium-
 117 doped yttrium aluminium garnet (Nd:YAG) laser that was of single pass design. The laser was
 118 precisely fired in synchronization with the RF of the cyclotron to pump the OPG-OPA laser.
 119 We based the OPG-OPA laser system on a continuous-wave (cw) external-cavity diode laser
 120 (ECDL) with a wavelength $\lambda \approx 1631$ nm. This seed beam was amplified using magnesium ox-
 121 ide doped periodically-polled lithium niobate (MgO:PPLN) crystals. This produced laser pulses
 122 of energy $E = 70$ uJ. OPA to $E = 10$ mJ was carried out in five potassium titanyl phosphate
 123 (KTP) crystals. The linewidth of the portion of the laser beam having a narrow spectral com-
 124 ponent was of order 10 GHz. These OPG and OPA processes introduced a 3 GHz uncertainty
 125 in the determination of the optical frequency of the laser pulses.

126 26.3 Experimental results

127 The experiments began by searching for the $(n, l) = (16, 15) \rightarrow (17, 14)$ transition by scanning
 128 a laser based on dye and Ti:Sapphire [53] pulse amplification over a 200 GHz wide region
 129 around the transition frequency $\nu_{\text{th}} = 781052.6(2.0)$ GHz which was calculated by theory [6].
 130 The 2.0 GHz uncertainty is caused in large part by the experimental uncertainty on the mass
 131 of π^- . No significant signal was observed. The coupling of the resonance daughter state
 132 $(n, \ell) = (17, 14)$ to an electronically excited state of $\pi^4\text{He}^+$ is theoretically expected to cause
 133 large scalar and tensor polarizabilities of amplitudes 4×10^4 and 70 atomic units, respectively

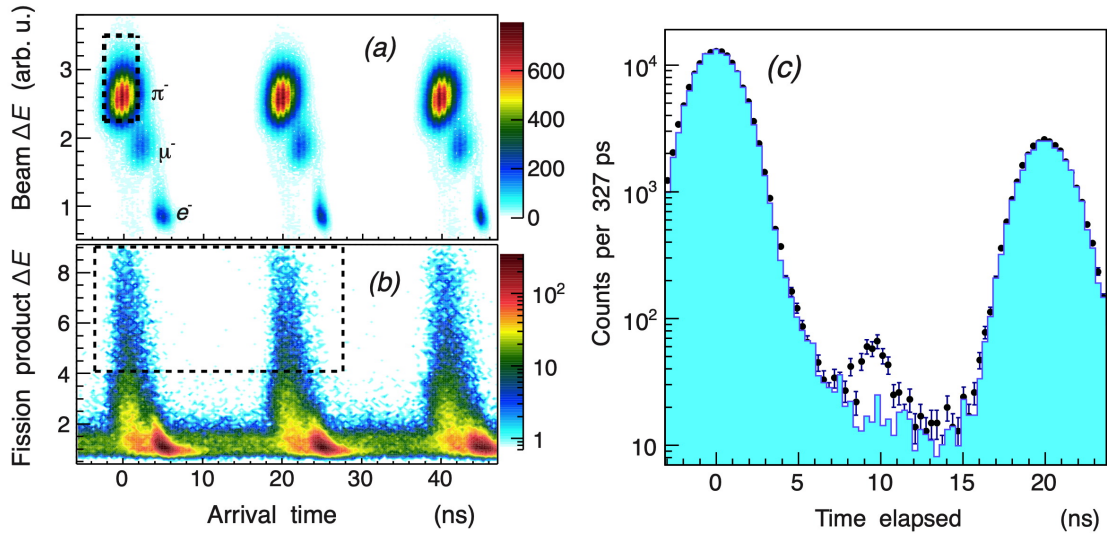


Figure 26.3: (a): A contour plot which shows the correlation between the arrival times t_a and the energy depositions ΔE of particles that were measured by a scintillation counter placed at the entrance of the helium target. The type of particle was identified. The π^- events in the rectangular region shown using broken lines were selected. (b): The $t_a - \Delta E$ plot of showing fission fragments that strike the scintillator array following π^- absorption by the helium nuclei. Background e^- with an energy deposition of $\Delta E < 20 - 25$ MeV were removed by accepting only the events in the region indicated by the rectangle. (c): The time spectra of nuclear fragments measured with (indicated by filled circles with error bars) and without (blue filled histogram) the laser irradiation at $t = 9$ ns. The peak in the former spectrum at $t = 9$ ns here corresponds to the laser resonance signal of $(17, 16) \rightarrow (17, 15)$. From [5].

134 [54], and this is believed to destabilize the daughter state against atomic collisions [55, 56].
 135 We next searched for the $(16, 15) \rightarrow (16, 14)$ resonance. The 250 fs lifetime [6] of the daughter
 136 state $(16, 14)$ should give rise to a large resonance width $\Gamma_A = 640$ GHz. Experimental data
 137 that corresponded to $> 6 \times 10^7$ detected π^- arrivals showed no signal that was statistically
 138 significant. The reason why the resonance was not observed is not understood. One possibility
 139 is that collisions with other helium atoms may destroy the π^- population that occupies the
 140 parent state $(n, \ell) = (16, 15)$. Similar effects have been observed in several states of $\bar{p}\text{He}^+$
 141 atoms [57–59]. Alternatively, it may be that only a negligible fraction of π^- are captured
 142 into state $(n, \ell) = (16, 15)$, as has been observed for some states of lower n in the $\bar{p}\text{He}^+$
 143 case [60–63].

144 We searched for the transition $(17, 16) \rightarrow (17, 15)$. The time spectrum indicated by filled cir-
 145 cles in Figure 26.3 (c) was measured by accumulating data from 2.5×10^7 π^- arrivals with the
 146 laser wavelength tuned to $\lambda \sim 1631.4$ nm. A peak was observed at $t \approx 9$ ns which contained
 147 some 300 events. The signal-to-noise ratio was 4 and the statistical significance > 7 standard
 148 deviations. Its width $\Delta t = 2$ ns was compatible with the expected dispersion of the time-of-
 149 flights of the fission fragments that arrive at the scintillator array. We found that the rate 3 h^{-1}
 150 of detected resonant $\pi^4\text{He}^+$ events is roughly compatible with the production rate $> 3 \times 10^5$
 151 s^{-1} of the atoms and with Monte Carlo simulations [6] that were carried out by assuming that
 152 most of the metastable population are captured into the parent state $(n, \ell) = (17, 16)$. When
 153 the laser was detuned off the resonance frequency (Figure 26.4 (a)-(d)), the signal proceeded
 154 to decrease and disappear.

155 The resonance signal intensity (Figure 26.4(a)–(d)) was obtained by taking the difference

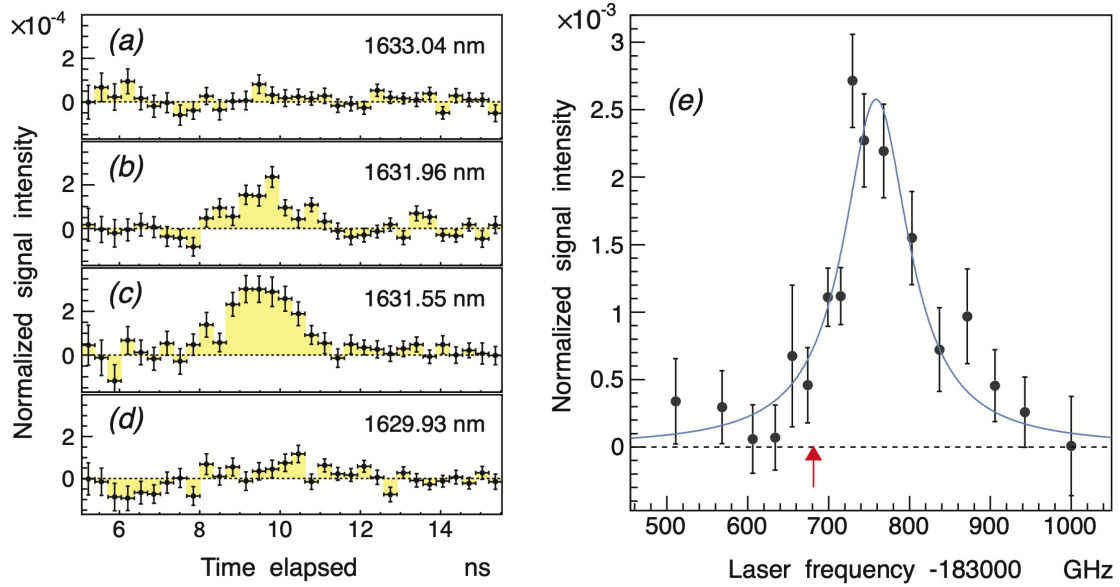


Figure 26.4: (a)–(d): The normalized time spectra of the resonance signal of the $\pi^4\text{He}^+$ transition $(n, l) = (17, 16) \rightarrow (17, 15)$ which was measured at four laser wavelengths. The spectra were obtained by taking the difference between the timing distributions of π^- absorption that were measured with and without the laser irradiation. (e): The profile of the resonance measured by scanning the laser frequency over a 500 GHz wide region, and then plotting the normalized counts under the peaks. From [5].

156 between the normalized time spectra that were measured with and without laser irradiation.
 157 The number of detected events under the induced peak around $t = 9$ ns was then counted. The
 158 resonance profile of Figure 26.4(e) was obtained by scanning the laser frequency. Each data
 159 point shown here contains data that were collected over a 20–30 h period of the experiment.
 160 The statistical uncertainty that arises from the finite number of $\pi^4\text{He}^+$ events is indicated
 161 by vertical error bars. The measured width of ≈ 100 GHz of this resonance agrees with a
 162 convolution of the expected 33 GHz Auger width [6] of the daughter state $(n, l) = (17, 15)$
 163 calculated by theory, collisional and power broadening [64] which are estimated to cause a
 164 contribution of ≈ 50 GHz, and the ≈ 10 GHz linewidth of the narrowband spectral component
 165 of the laser pulses. Some further broadening of this resonance may be caused by atomic
 166 collisions that shorten [54, 57] the lifetime of the resonance daughter state $(n, l) = (17, 15)$.
 167 The spacing of 3.0 GHz [6, 65] between the fine structure sublines that is expected from the
 168 interaction between the electron spin and the orbital angular momentum of π^- cannot be
 169 resolved in our experiment since it is much smaller than the 33 GHz natural width of the
 170 resonance itself. The best fit (see blue curve) of two overlapping Lorentzian functions which
 171 take these sublines into account was shown to have a reduced χ^2 value of 1.0. The resonance
 172 centroid is $\nu_{\text{exp}} = 183760(6)(6)$ GHz. The statistical uncertainty of 6 GHz is due to the finite
 173 number of detected $\pi^4\text{He}^+$. The systematic uncertainty of 6 GHz contains the contribution of
 174 5 GHz that is related to the selection of this fit function as well as other contributions related
 175 to the laser.

176 This ν_{exp} value determined in the experiment is larger by $\Delta\nu = (78 \pm 8)$ GHz compared
 177 to the theoretical value [6] $\nu_{\text{th}} = (183681.8 \pm 0.5)$ GHz. This shift in the resonance frequency
 178 is believed to be caused by collisions with other helium atoms [64]. Some similar effects have

179 been previously observed [57, 66] for some $\bar{p}\text{He}^+$ resonances. The gradient of this shift that is
 180 expected at a target temperature $T = 4$ K was calculated to be $d\nu/d\rho = (4.4 - 6.5) \times 10^{-21}$
 181 $\text{GHz}\cdot\text{cm}^3$ using the impact approximation of the binary collision theory of spectral lineshapes
 182 [64]. At the density of the superfluid target used in these experiments, the blueshift expected
 183 from theory corresponds to between $\Delta\nu = 96$ and 142 GHz. This theoretical result roughly
 184 agrees with the result of the experiment. This collisional shift must be experimentally mea-
 185 sured before the π^- mass can be determined.

186 In future experiments in PSI, we are planning to search for other transitions such as
 187 $(n, l) = (17, 16) \rightarrow (16, 15)$ that should be narrower by a factor of at least 10^{-3} compared to
 188 the recently-detected transition using helium gas targets where the collisional shifts are small.
 189 The precision of ν_{th} is now limited by the experimental uncertainty of the π^- mass, but the
 190 precision of the calculations themselves [6] can be improved to a fractional precision of less
 191 than 10^{-8} for some transitions as in the HD^+ [67, 68] and $\bar{p}\text{He}^+$ [16, 17] cases. These pionic
 192 experiments at PSI will also complement the measurements on $\bar{p}\text{He}^+$ that will be carried out
 193 at the ELENA and Antiproton Decelerator facilities [69, 70].

194 References

- 195 [1] G. T. Condo, *On the absorption of negative pions by liquid helium*, Phys. Lett. **9**(1), 65
 196 (1964).
- 197 [2] J. E. Russell, *Metastable states of $\alpha\pi^-e^-$, αK^-e^- , and $\alpha\bar{p}e^-$ atoms*, Phys. Rev. Lett. **23**(2),
 198 63 (1969).
- 199 [3] J. E. Russell, *Structure of neutral mesonic atoms formed in liquid helium*, Phys. Rev. A
 200 **1**(3), 721 (1970).
- 201 [4] J. E. Russell, *Auger rates for circular orbits of $\alpha\pi^-e^-$, αK^-e^- , and $\alpha\bar{p}e^-$ atoms*, Phys. Rev.
 202 A **1**(3), 742 (1970).
- 203 [5] M. Hori, H. Aghai-Khozani, A. Sótér, A. Dax and D. Barna, *Laser spectroscopy of pionic*
 204 *helium atoms*, Nature **581**, 37 (2020).
- 205 [6] M. Hori, A. Sótér and V. I. Korobov, *Proposed method for laser spectroscopy of pionic helium*
 206 *atoms to determine the charged-pion mass*, Phys. Rev. A **89**, 042515 (2014).
- 207 [7] S. Lenz *et al.*, *A new determination of the mass of the charged pion*, Phys. Lett. B **416**(1-2),
 208 50 (1998).
- 209 [8] M. Trassinelli *et al.*, *Measurement of the charged pion mass using X-ray spectroscopy of*
 210 *exotic atoms*, Phys. Lett. B **759**, 583 (2016).
- 211 [9] M. Daum, R. Frosch and P.-R. Kettle, *The charged and neutral pion masses revisited*, Phys.
 212 Lett. B **796**, 11 (2019).
- 213 [10] K. Assamagan *et al.*, *Upper limit of the muon-neutrino mass and charged-pion mass from*
 214 *momentum analysis of a surface muon beam*, Phys. Rev. D **53**(11), 6065 (1996).
- 215 [11] E. Salumbides, W. Ubachs and V. I. Korobov, *Bounds on fifth forces at the sub-Å length*
 216 *scale*, J. Mol. Spectrosc. **300**, 65 (2014).
- 217 [12] J. Murata and S. Tanaka, *A review of short-range gravity experiments in the LHC era*, Class.
 218 Quantum Gravity **32**(3), 033001 (2015).

- 219 [13] F. Ficek *et al.*, *Constraints on exotic spin-dependent interactions between matter and anti-*
220 *matter from antiprotonic helium spectroscopy*, Phys. Rev. Lett. **120**(18), 183002 (2018).
- 221 [14] A. S. Lemos, G. C. Luna, E. Maciel and F. Dahia, *Spectroscopic tests for short-range mod-*
222 *ifications of Newtonian and post-Newtonian potentials*, Class. Quantum Gravity **36**(24),
223 245021 (2019).
- 224 [15] J. Ding *et al.*, *Constraints on the velocity and spin dependent exotic interaction at the*
225 *micrometer range*, Phys. Rev. Lett. **124**(16), 161801 (2020).
- 226 [16] V. I. Korobov, L. Hilico and J.-P. Karr, *$m\alpha^7$ -order corrections in the hydrogen molecular*
227 *ions and antiprotonic helium*, Phys. Rev. Lett. **112**(10), 103003 (2014).
- 228 [17] V. Korobov, L. Hilico and J.-P. Karr, *Theoretical transition frequencies beyond 0.1 ppb*
229 *accuracy in H_2^+ , HD^+ , and antiprotonic helium*, Phys. Rev. A **89**(3), 032511 (2014).
- 230 [18] V. I. Korobov, *Bethe logarithm for resonant states: Antiprotonic helium*, Phys. Rev. A **89**(1),
231 014501 (2014).
- 232 [19] M. Hori *et al.*, *Two-photon laser spectroscopy of antiprotonic helium and the antiproton-*
233 *to-electron mass ratio*, Nature **475**, 484 (2011).
- 234 [20] M. Hori *et al.*, *Buffer-gas cooling of antiprotonic helium to 1.5 to 1.7 K, and antiproton-*
235 *to-electron mass ratio*, Science **354**(6312), 610 (2016).
- 236 [21] A. Adamczak and D. Bakalov, *Shift and broadening of resonance lines of antiprotonic*
237 *helium atoms in liquid ^4He* , Phys. Rev. A **88**(4), 042505 (2013).
- 238 [22] M.-H. Hu, S.-M. Yao, Y. Wang, W. Li, Y.-Y. Gu and Z.-X. Zhong, *Variational calculation*
239 *of energy levels for metastable states of antiprotonic helium*, Chem. Phys. Lett. **654**, 114
240 (2016).
- 241 [23] D. T. Aznabaev, A. K. Bekbaev and V. I. Korobov, *Nonrelativistic energy levels of helium*
242 *atoms*, Phys. Rev. A **98**(1), 012510 (2018).
- 243 [24] D. Baye, J. Dohet-Eraly and P. Schoofs, *Structure changes along the lowest rotational band*
244 *of the antiprotonic helium atom*, Phys. Rev. A **99**(2), 022508 (2019).
- 245 [25] Z.-D. Bai, Z.-X. Zhong, Z.-C. Yan and T.-Y. Shi, *Complex coordinate rotation method based*
246 *on gradient optimization*, Chin. Phys. B (2020).
- 247 [26] T. P. Grozdanov and E. A. Solov'ev, *Hidden-crossing explanation of frozen-planet resonances*
248 *in antiprotonic helium; their positions and widths*, Eur. Phys. J. D **74**(3), 50 (2020).
- 249 [27] J. Koch and F. Scheck, *Quadrupole interactions in pionic and kaonic atoms*, Nucl. Phys. A
250 **340**(2), 221 (1980).
- 251 [28] M. Trassinelli and P. Indelicato, *Relativistic calculations of pionic and kaonic atoms' hyper-*
252 *fine structure*, Phys. Rev. A **76**(1), 012510 (2007).
- 253 [29] J. G. Fetkovich and E. G. Pewitt, *Experimental study of the cascade time of negative mesons*
254 *in a liquid helium bubble chamber*, Phys. Rev. Lett. **11**(6), 290 (1963).
- 255 [30] M. M. Block *et al.*, *Moderation time for nuclear capture of negative pions in liquid He^4* ,
256 Phys. Rev. Lett. **11**(6), 301 (1963).

- 257 [31] M. M. Block, J. B. Kopelman and C. R. Sun, *Moderation and cascade times of negative*
258 *pions and negative kaons in liquid helium*, Phys. Rev. **140**(1B), B143 (1965).
- 259 [32] O. A. Zaimidoroga, R. M. Sulyaev and V. M. Tsupko-Sitnikov, *Measurement of the pi-meson*
260 *cascade transition time in gaseous He³*, Soviet Journal of Experimental and Theoretical
261 Physics **25**, 63 (1967).
- 262 [33] S. N. Nakamura *et al.*, *Negative-pion trapping by a metastable state in liquid helium*, Phys.
263 Rev. A **45**(9), 6202 (1992).
- 264 [34] H. L. Anderson, J. Marshall, L. Kornblith Jr, L. Schwarcz and R. Miller, *Synchrocyclotron*
265 *for 450-MeV protons*, Rev. Sci. Instrum. **23**(12), 707 (1952).
- 266 [35] J. Ashkin, J. P. Blaser, F. Feiner, J. G. Gorman and M. O. Stern, *Total cross sections for*
267 *negative and positive pions in hydrogen and deuterium*, Phys. Rev. **96**(4), 1104 (1954).
- 268 [36] R. J. Walker *et al.*, *The Northwestern University 50 cm liquid helium bubble chamber*, Rev.
269 Sci. Instrum. **39**(10), 1407 (1968).
- 270 [37] G. Backenstoss *et al.*, *Pionic and muonic x-ray transitions in liquid helium*, Nucl. Phys. A
271 **232**(2), 519 (1974).
- 272 [38] R. Landua and E. Klempt, *Atomic cascade of muonic and pionic helium atoms*, Phys. Rev.
273 Lett. **48**(25), 1722 (1982).
- 274 [39] D. Gotta, *Precision spectroscopy of light exotic atoms*, Prog. Part. Nucl. Phys. **52**(1), 133
275 (2004).
- 276 [40] M. Hori *et al.*, *Observation of cold, long-lived antiprotonic helium ions*, Phys. Rev. Lett.
277 **94**(6), 063401 (2005).
- 278 [41] G. Y. Korenman and S. Yudin, *Neutralization of excited antiprotonic helium ion in collisions*
279 *with helium atoms*, arXiv preprint arXiv:1912.00507 (2019).
- 280 [42] R. Abela, F. Foroughi and D. Renker, *Muon beams at PSI*, Z. Phys. C **56**(1), S240 (1992).
- 281 [43] E. Daum *et al.*, *Pion absorption at rest in ⁴He*, Nucl. Phys. A **589**(4), 553 (1995).
- 282 [44] C. Cernigoi *et al.*, *Energy spectra of single neutrons and charged particles emitted following*
283 *the absorption of stopped negative pions in ⁴He*, Nucl. Phys. A **352**(3), 343 (1981).
- 284 [45] A. Sótér *et al.*, *Segmented scintillation detectors with silicon photomultiplier readout for*
285 *measuring antiproton annihilations*, Rev. Sci. Instrum. **85**(2), 023302 (2014).
- 286 [46] K. Todoroki *et al.*, *Instrumentation for measurement of in-flight annihilations of 130 keV*
287 *antiprotons on thin target foils*, Nucl. Instr. and Meth. A **835**, 110 (2016).
- 288 [47] Y. Murakami, H. Aghai-Khozani and M. Hori, *Lead fluoride Cherenkov detector read out*
289 *by avalanche photodiodes for measuring the intensities of pulsed antiproton beams*, Nucl.
290 Instrum. and Meth. A **933**, 75 (2019).
- 291 [48] S. Ritt, R. Dinapoli and U. Hartmann, *Application of the DRS chip for fast waveform*
292 *digitizing*, Nucl. Instrum. and Meth. A **623**(1), 486 (2010).
- 293 [49] H. Friederich *et al.*, *A scalable DAQ system based on the DRS4 waveform digitizing chip*,
294 IEEE Trans. Nucl. Sci. **58**(4), 1652 (2011).

- 295 [50] H. Aghai-Khozani *et al.*, *First experimental detection of antiproton in-flight annihilation*
296 *on nuclei at ~ 130 keV*, *Eur. Phys. J. Plus* **127**(10), 125 (2012).
- 297 [51] A. Bianconi *et al.*, *Measurement of the antiproton–nucleus annihilation cross section at 5.3*
298 *MeV*, *Phys. Lett. B* **704**(5), 461 (2011).
- 299 [52] H. Aghai-Khozani *et al.*, *Measurement of the antiproton–nucleus annihilation cross-section*
300 *at low energy*, *Nucl. Phys. A* **970**, 366 (2018).
- 301 [53] M. Hori and A. Dax, *Chirp-corrected, nanosecond Ti:sapphire laser with 6 MHz linewidth*
302 *for spectroscopy of antiprotonic helium*, *Opt. Lett.* **34**(8), 1273 (2009).
- 303 [54] V. I. Korobov, A. K. Bekbaev, D. T. Aznabayev and S. A. Zhaugasheva, *Polarizability of the*
304 *pionic helium atom*, *J. Phys. B* **48**(24), 245006 (2015).
- 305 [55] O. I. Kartavtsev, D. E. Monakhov and S. I. Fedotov, *Auger decay rates of antiprotonic*
306 *helium*, *Phys. Rev. A* **61**(6), 062507 (2000).
- 307 [56] H. Yamaguchi *et al.*, *Anomalies in the decay rates of antiprotonic helium-atom states*, *Phys.*
308 *Rev. A* **66**(2), 022504 (2002).
- 309 [57] M. Hori *et al.*, *Sub-ppm laser spectroscopy of antiprotonic helium and a CPT-violation limit*
310 *on the antiprotonic charge and mass*, *Phys. Rev. Lett.* **87**(9), 093401 (2001).
- 311 [58] T. Kobayashi *et al.*, *Observation of the 1154.9 nm transition of antiprotonic helium*, *J.*
312 *Phys. B* **46**(24), 245004 (2013).
- 313 [59] V. I. Korobov, Z.-X. Zhong and Q.-L. Tian, *Leading term of the $\bar{p}\text{He}^+$ long-range interaction*,
314 *Phys. Rev. A* **92**(5), 052517 (2015).
- 315 [60] M. Hori *et al.*, *Primary populations of metastable antiprotonic ^4He and ^3He atoms*, *Phys.*
316 *Rev. Lett.* **89**(9), 093401 (2002).
- 317 [61] M. Hori *et al.*, *Populations and lifetimes in the $\nu = n - \ell - 1 = 2$ and 3 metastable cascades*
318 *of $\bar{p}\text{He}^+$ measured by pulsed and continuous antiproton beams*, *Phys. Rev. A* **70**(1), 012504
319 (2004).
- 320 [62] J. S. Cohen, *Capture of negative exotic particles by atoms, ions and molecules*, *Rep. Prog.*
321 *Phys.* **67**(10), 1769 (2004).
- 322 [63] K. Sakimoto, *Formation of antiprotonic helium $\bar{p}\text{He}^+$ and ionization in low-energy colli-*
323 *sions of \bar{p} with He in the ground 1^1S and metastable 2^3S and 2^1S states*, *Phys. Rev. A*
324 **91**(4), 042502 (2015).
- 325 [64] B. Obreshkov and D. Bakalov, *Collisional shift and broadening of the transition lines in*
326 *pionic helium*, *Phys. Rev. A* **93**(6), 062505 (2016).
- 327 [65] S. Friedreich *et al.*, *Microwave spectroscopic study of the hyperfine structure of antiprotonic*
328 *^3He* , *J. Phys. B* **46**(12), 125003 (2013).
- 329 [66] D. Bakalov, B. Jeziorski, T. Korona, K. Szalewicz and E. Tchoukova, *Density shift and*
330 *broadening of transition lines in antiprotonic helium*, *Phys. Rev. Lett.* **84**(11), 2350 (2000).
- 331 [67] S. Alighanbari, G. S. Giri, F. L. Constantin, V. I. Korobov and S. Schiller, *Precise test*
332 *of quantum electrodynamics and determination of fundamental constants with HD^+ ions*,
333 *Nature* **581**, 152 (2020).

- 334 [68] S. Patra *et al.*, *Proton-electron mass ratio from laser spectroscopy of HD^+ at the part-per-*
335 *trillion level*, *Science* **369**(6508), 1238 (2020).
- 336 [69] V. Chohan *et al.*, *Extra low energy antiproton (ELENA) ring and its transfer lines: Design*
337 *report*, CERN-2014-002, Geneva, Switzerland (2014).
- 338 [70] M. Hori and J. Walz, *Physics at CERN's Antiproton Decelerator*, *Prog. Part. Nucl. Phys.* **72**,
339 206 (2013).